SRI International

Final Report 3 • 28 February 2003

OBSERVATIONS AND SIMULATIONS OF THE M–I COUPLING OF BURSTY CONVECTION

SRI Project No. P10055

Prepared by
Ennio R. Sánchez, Senior Research Physicist
Engineering and Systems Division

Prepared for:
DCMC-SF-Sacramento
1380 Leadhill Boulevard, Suite 260
Roseville, CA 95661-2941

Grant NAG5-8111

Approved
John Kelly, Program Director
Engineering and Systems Division

333 Ravenswood Avenue • Menlo Park, CA 94025-3493 • (650) 859-2000

CONTENTS

FIGURES

1 INTRODUCTION

This final report summarizes the development and application of the first ever method to measure a proxy of the global merging along the solar wind–Earth separatrix. This work was performed under NASA Grant NAG5-8111, "Observations and Simulations of the M–I Coupling of Bursty Convection."

The ultimate aim of the project is to quantify the reconnection potential in the magnetotail and the fraction of it that is due to bursty bulk flows (BBFs). To achieve this goal, we developed the first method that allows the measurement of the distribution of reconnection rate along the polar cap boundary. The method was then applied to substorms and steady magnetospheric convection (labeled as SMC or convection bay) periods in order to quantify the strength of reconnection and the fraction of it that is contributed by BBFs in each case. Results of this research were reported in two manuscripts submitted to the *Journal of Geophysical Research* and presented at three international conferences.

This report is organized as follows. In Section 2 we discuss the conceptual framework that is the foundation of the method. In Section 3 we describe the details of the method. In Section 4 we describe the application of the technique to substorms and SMCs. In Section 5 we summarize the results of this investigation and provide references to the manuscripts and conference presentations that report on the results of this project.

2 CONCEPTUAL FRAMEWORK

The circulation of mass energy and momentum in the Earth's magnetosphere is driven by an electric potential imposed by the electrodynamic coupling between the solar wind and the magnetosphere–ionosphere (M–I) system. The magnitude of the potential is essentially directly proportional to the rate at which the solar wind magnetic field merges with the Earth's magnetic field per unit length on the dayside magnetopause [e.g., Reiff and Luhmann, 1986]. The prediction of mass, energy, and momentum circulation in the Earth's magnetosphere is one of the main objectives of the Sun-Earth Connection Roadmap and is accordingly one of four stated objectives of the Sun-Earth Connection Guest Investigator Program.

In a statistical sense, the average conversion of closed to open magnetic flux is balanced by the conversion of open to closed flux, as expected for a long-term magnetic flux balance in the magnetosphere or in steady state. However, dayside and nightside merging rates are expected to be different for a large number of solar wind conditions and timescales [e.g., Lockwood et al., 1990; Cowley and Lockwood, 1992]. Therefore, a quantification of the temporal and spatial variation of the global merging rates during the entire range of solar wind conditions is a fundamental step to establish a relationship between the general circulation in the magnetosphere and solar wind input that can be compared with predictions of large-scale circulation models of the magnetosphere. However, before we can claim that the general circulation of the magnetosphere can be predicted from first principles for any given solar wind input, we must have the ability to predict two fundamental magnetospheric quantities: (1) the cycle of magnetic field merging—that is, how much IMF (interplanetary magnetic field) leaks through the boundary between the solar wind and the magnetosphere, how much magnetic flux accumulates in the magnetotail, and how much of this flux merges again in the magnetotail; and (2) a macroscopic description of the general circulation in the magnetosphere.

We addressed the first question in the paper "A new method to measure global reconnection in the Earth's magnetosphere" [Sánchez et al., 2003a]. In that paper we developed a method that combines global measurements of the polar cap boundary with global estimates of the polar cap potential distribution to quantify the net magnetic field merging rate. Large-scale circulation models of the magnetosphere have the underlying assumption that magnetic merging at the dayside magnetospheric boundary makes the open field line polar cap expand; nightside magnetic merging in the tail makes it contract. If the dayside merging rate exceeds the nightside merging rate, there is net expansion of the polar cap boundary (the so-called polar cap inflation). If the nightside merging rate exceeds the dayside merging rate, there is contraction (termed polar cap deflation) [Siscoe and Huang, 1985]. In the ionosphere, measuring merging rate is equivalent to measuring the amount of magnetic flux converted from closed to open or open to closed in units of Wb/s, which is the same as volts. Hence, measurement of merging rates in the ionosphere requires measuring the electric field potential across the line onto which the magnetospheric merging line projects. We compare merging rates with the inflation rate of the polar cap to establish a measure of consistency of independent estimates of flux transport across the polar cap boundary and to estimate the deviation of the M–I coupling from steady state for a range of solar wind inputs.

We determine a proxy of the global merging rate at the Earth's magnetopause by calculating the magnetic flux transport across the polar cap boundary. Then we can compare the rate of magnetic flux transfer across the polar cap boundary with the inflation and deflation of the polar cap to establish a measure of consistency of independent estimates of flux transport across the polar cap boundary.

The relationship between magnetic field merging and circulation of mass and magnetic flux in the Earth's magnetosphere is a link of crucial importance in the Sun-Earth connection research. In recent years it has become increasingly clear that a significant portion of the transport of energy and magnetic flux in the magnetotail is, for some fraction of the time, likely to be accomplished via high-speed flows within the plasma sheet which last a few minutes [Baumjohann et al., 1989,1990; Angelopoulos et al., 1992]. These flows have a characteristic duration of 10 min and a substructure of 1 min. The 10 min timescale structures are termed bursty bulk flows, and the 1 min structures are called flow bursts. Flow bursts correlate positively with magnetic field dipolarizations and ion temperature increases. The importance of the fast flows for transport of energy and magnetic flux in the magnetotail has become apparent from a number of studies using Active Magnetosphere Particle Tracer Explorer (AMPTE), International Sun Earth Explorer (ISEE), and International Solar Terrestrial Physics (ISTP) observations.

Statistical studies find that BBFs are responsible for 60 to 100 percent of the measured earthward mass energy and magnetic flux transport past the satellite in the high-beta plasma sheet, despite being observed only 10 to 15 percent of the time in the midnight plasma sheet [Angelopoulos et al., 1994]. Multipoint measurements suggest that flow bursts are confined to narrow channels with a YZ extent of a few R_e[2] [Angelopoulos et al., 1996,1997] and approximately 20 R_e or more length in X.

Other observations have found a link between earthward flow bursts observed near the midnight central plasma sheet by Geotail and auroral intensifications at the polar cap boundary (termed separatrix disturbances) observed by the CANOPUS ground-based array in central Canada [e.g., Lyons et al., 1999]. These observations show that the plasma sheet has considerable structure and bursty flow activity in the sampled range ($-30\ R_e < X_{GSM} < -12\ R_e$) when separatrix disturbances occur. Conversely, the plasma sheet is more uniform in structure and convection properties during periods when significant separatrix disturbances were not seen. This is consistent with the separatrix disturbance being the result of the mapping to the ionosphere of the electric field that gives rise to bursty flows within the plasma sheet. The ion phase space distributions are of the type expected from Speiser motion in thin plasma sheet regions suggesting that the bursty flows are within temporally and spatially localized regions where the plasma sheet is significantly thinner than elsewhere. These localized regions appear also to be regions of enhanced electric field associated with similarly localized regions of enhanced reconnection; neither dipolarizations of the large-scale magnetic field nor reductions in total plasma sheet pressure are seen in association with the separatrix disturbances. These properties are frequently observed during SMC periods [see Sergeev et al., 1996].

3 METHOD FOR CALCULATION OF RECONNECTION

The calculation of merging rates requires the knowledge of the polar cap boundary orientation, latitude, and velocity as well as the distribution of high-latitude electric field. In this section we describe in detail the method used to calculate each of these quantities. Then we describe an example of the application of the technique for the calculation of nightside merging rate and its relationship to polar cap inflation. Finally, we describe a method to relate measured merging rates to plasma transport rate in the plasma sheet.

3.1 CALCULATION OF THE POLAR CAP BOUNDARY FROM POLAR UVI MEASUREMENTS

Polar LBH-L UVI images are processed from detector counts to an equivalent photometric flux (photons/cm^2 s) and rendered on georegistered grids of latitude and longitude. Subsequent processing includes correction for scattered solar UV on the dayside, magnetic mapping, and a harmonic fit for a poleward boundary corresponding to a fixed emission threshold of 1.5 to 4.5 photons/cm^2 s. Images are uncorrected for POLAR UVI platform wobble.

All images used to calculate a merging electric field are from apogee passes with a relatively high viewing angle of the auroral oval. With such a geometry, scattered solar UV can be approximated by a low-order function of solar zenith angle (SZA). Our processing program examines the dayside subauroral emission for each LBH-L image to determine such a function. In order to suppress spurious image noise, three 37 s images are averaged prior to extraction of the subauroral dayside brightness data. The resulting sunlit component is scaled against the known SZA array to determine a best-fit analytic proxy for scattered sunlight. This scattered solar UV model image is subsequently subtracted from each image. Each image is then mapped to magnetic coordinates using the PACE model [Baker and Wing, 1989] at an assumed emission altitude of 110 km.

Magnetically mapped and solar corrected images are then examined for the location of the polar boundary of the auroral oval. LBHL-L images are proportional to the incident energy flux of auroral electron precipitation [Torr et al., 1995] and thus a selection of emission threshold, or emission gradient is equivalent to specifying a threshold or gradient in energy flux. Polar boundaries defined over our emission range, corresponding to energy fluxes of ~5 to 20 mW m^{-2}, are in the range expected at the edge of the instantaneous auroral boundary as identified by incoherent-scatter radar (ISR) [Doe et al., 1997].

On an individual image-by-image basis, the identified emission threshold is analytically fit with 6th order harmonic function, corresponding to a local time resolution of 4 hours. An analysis of two examples from the winter of 1998 (14–15 February and 3–4 February) has revealed little difference in fitting the boundary at a threshold of 1.5 photons/cm^2 s or the value of 4.3 photons/ cm^2 s recommended for nightside boundary identification by Baker et al. [2000], suggesting that for these case study events, the LBH-L emission gradients are quite large at the polar cap boundary. Subsequent to fitting, the time history of this boundary is examined to isolate position, azimuthal tilt, and instantaneous velocity of the polar cap boundary required for calculation of nightside merging potential. Newell et al. [1996] note that a polar cap boundary (b5e) based on DMSP SSJ/4 electron spectra can be located reliably by isolating energy flux changes of a factor

of four over a 12 s (~800 km) sample period. A gradient of this magnitude is similar to the energy flux gradient found for the polar cap boundary in our reconnection case study of LBH-L images. A cursory review of February 1998 POLAR UVI images coincident with DMSP overflights indicates that LBH-L images underestimate the latitude of the polar cap boundary, relative to the Newell et al. [1996] b5e, by 1 to 3 deg. A slightly larger UV/DMSP underestimate was quantified with comparison of Viking satellite LBH band auroral boundaries and the b5e boundary by Kauristie et al. [1999]. In their study, the LBH band images responded to both energy flux and characteristic energy of auroral electron precipitation, and thus should not be expected to agree with the b5e boundary definition. The Viking UV image integration time of 60 s may also have introduced significant temporal and spatial smoothing with respect to the 12 s b5e identification period. A more significant source of uncertainty in our current data set is likely the effect of platform wobble, worst case estimated at 4 deg by Baker et al. [2000].

3.2 MEASUREMENT OF IONOSPHERIC ELECTRIC FIELD DISTRIBUTION

Given the knowledge of the polar cap boundary location, orientation, and velocity, the next step toward the quantification of merging and reconnection rates is the measurement of the electric field distribution in the high latitude ionosphere. A first approximation of the electric field distribution is obtained from the actual vector radar measurements. Electric field vectors are obtained from incoherent-scatter and SuperDARN radars. We apply the JHU/APL Spherical Harmonic Fitting (SHF) [Ruohoniemi and Greenwald, 1996; Ruohoniemi and Baker, 1998] to determine the global electric field distribution. In this method, the two-dimensional velocity at a point is unambiguously resolved at the gridpoints where two or more radars make simultaneous measurements. However, all available line of sight velocity data serve to constrain the possibilities for the large-scale convection pattern. The pattern that is most consistent with the measurements can be determined by a spherical harmonic series expansion,

$$\Phi(\theta, \phi) = \sum_{l=0}^{L} \sum_{m=-M}^{M} A_{lm} Y_{lm}(\theta, \phi) \quad ,$$

where A_{lm} are complex valued coefficients and L and M are the order and degree of the expansion, respectively, with $M \leq L$.

The relations between the electrostatic potential, convection electric field, and velocity are given by

$$\mathbf{E} = -\nabla\Phi \qquad \mathbf{V} = \frac{\mathbf{E} x \mathbf{B}}{B^2} \quad .$$

The filtered line of sight velocity values have been converted to the mapping grid, furnishing a set of N velocity values and their uncertainties, W_i and σ_i. The quantity to be minimized is

$$\chi^2 = \sum_{i=1}^{N} \frac{1}{\sigma_i^2} \left[\mathbf{V}[i] \bullet \hat{\mathbf{k}}[i] - W_i \right]^2 \quad ,$$

The product $\mathbf{V}[i] \bullet \hat{\mathbf{k}}[i]$ provides the projection of the velocity onto the line of sight direction. The values of L and M determine the spatial filtering performed on the velocity data. In the fits, initially we will use L=6 and M=6, which provides a resolution of 30 deg in longitude and 2.5 deg in latitude, and will assume the zero potential boundary at 60 deg latitude. Adjustments

to these parameters can be easily introduced in the fitting procedure depending on the spatial scale of the structure in the aurora observed in the POLAR images.

The fitting procedure can be applied directly to any set of velocity data to find a set of coefficients that reproduces the input values as nearly as possible according to the minimum χ^2 criterion. In principle, a set of coefficients can be solved for Φ over the entire polar grid. This amounts to the extrapolation of the fitting solution obtained over the area covered by measurements to the undersampled portions of the polar region. One approach is to extrapolate the undersampled region by folding in velocity information from a statistical convection model (for instance, the APL model of Ruohoniemi and Greenwald [1996]). The result is a global convection pattern with a high degree of confidence in the area with available measurements and decreased confidence in relation to how much a region is undersampled. Therefore, we only calculate merging rates along the polar cap segments where radar measurements are available. We calculate a net merging rate from the integral of the tangential electric field only when there are sufficient radar measurements covering dayside and nightside merging regions simultaneously.

The merging rate resulting from calculating a tangential electric field along the entire polar cap boundary when radar sampling of one of the merging regions is not available will be used only as a measure of the deviation of the net merging from the steady state assumption. For example, if there is sufficient radar data to estimate the nightside merging potential, then the deviation from zero of the total potential resulting from integrating along the entire polar cap boundary will be used as an estimation of how much the dayside reconnection potential deviates from a balanced merging.

3.3 CALCULATION OF MERGING RATES

The measurement of merging rates is based on the same application principles that were used by Vasyliunas [1984] and applied to local merging calculations by Blanchard et al. [1996,2001]. The time rate of change of magnetic flux through a loop on the separatrix, defined as the surface that separates open from closed field lines and connects the merging line in the magnetosphere with the polar cap boundary, is

$$\Phi_M = \frac{\partial}{\partial t}\int \vec{B} \bullet d\hat{a} = \oint d\vec{\ell} \bullet \left(\vec{E} + \vec{U} \times \vec{B}\right) ,$$

where the line integral is performed over a loop that contains a segment of the polar cap boundary on one end and a segment of the X-line on the other, and is completed by magnetic field lines that lie on the separatrix and connect the edges of both segments. Choosing a loop that lies entirely on the separatrix ensures that Φ_M is zero, since $\vec{B} \bullet d\hat{a} = 0$. Then the following relation holds:

$$\oint d\vec{\ell} \bullet \left(\vec{E} + \vec{U} \times \vec{B}\right) = 0$$

The integral can be written as the sum of the integral along the X-line, the integral along the polar cap boundary, and the integral on the rest of the loop.

For the loop element along the X-line, $d\vec{\ell} \bullet \vec{U} \times \vec{B} = 0$ and therefore

$$\int_{Xline} d\vec{\ell} \bullet \left(\vec{E} + \vec{U} \times \vec{B}\right) = \int_{Xline} d\vec{\ell} \bullet \vec{E} \ .$$

The integral along the polar cap boundary can be written as

$$\int_{PCB} d\vec{\ell} \bullet \vec{B}_i \times \left(\vec{V}_n - \vec{U}_n\right) \ .$$

The merging electric field in the frame of reference of the polar cap boundary is therefore given at each point along the boundary by the relationship

$$\vec{E}_{merge} = \vec{B}_i \times \left(\vec{V}_n - \vec{U}_n\right) \ ,$$

where $\vec{V}_n$ is the ionospheric plasma flow normal to the polar cap boundary, $\vec{U}_n$ is the normal velocity component of the polar cap boundary, and $\vec{B}_i$ is the ambient magnetic field in the ionosphere. The integral on the Faraday loop can then be written as

$$\int_{Xline} d\vec{\ell} \bullet \vec{E} = \int_{PCB} d\vec{\ell} \bullet \vec{E}_{merge} + \int_{\substack{restof \\ loop}} d\vec{\ell} \times \vec{B} \bullet \left(\vec{U} - \vec{V}\right) \ .$$

Therefore, the integral of the electric field along the polar cap boundary gives the rate of magnetic flux transfer across the polar cap boundary.

The merging potential along the X-line is equivalent to the potential along the polar cap boundary to the extent that the integral along the rest of the loop is negligible. The goodness of this approximation depends on the validity of the MHD approximation $\vec{E} = -\vec{V}x\vec{B}$ for the component of the electric field tangential to the separatrix and normal to the magnetic field along the polar cap boundary. It also implies that any magnetic field-aligned potential drops along the magnetic field that defines a separatrix has the same magnitude as the potential drop on the other edge of the separatrix.

Figure 1 is a schematic view of the length vector element convention used for the calculation of the merging potential. According to this convention, a positive value of the integral of the electric field along a segment of the polar cap boundary corresponds to net flux from the oval into the polar cap over that segment. A negative value represents net flux into the oval.

Define the net rate of magnetic flux transfer across the polar cap boundary as

$$\Phi_{net} = \int \vec{E}_{rec} \cdot \vec{dl}$$

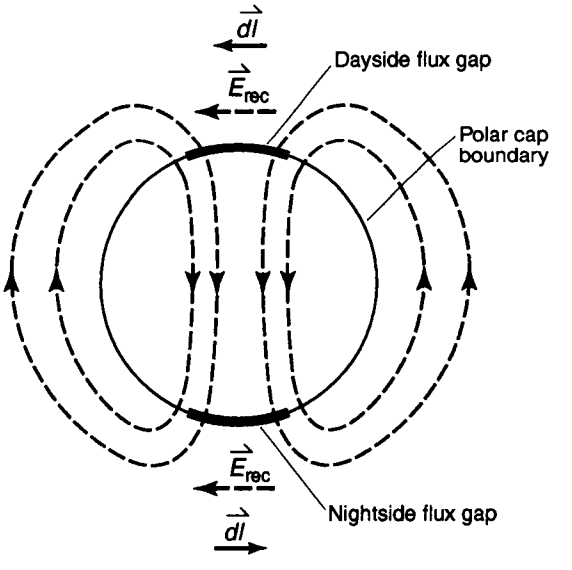

Figure 1. Schematic showing calculation of merging and reconnection rates along polar cap boundary.

4 RECONNECTION CALCULATION FOR SUBSTORMS AND SMCS

We applied the merging calculation technique for a substorm period on 14 February 1998 and a five-hour interval of near steady southward IMF on 15 February [Sánchez et al., 1999,2000, 2001,2003a,2003b]. Continuous view of the full oval by POLAR UVI was available during the entire observation period. Therefore, POLAR images were used to calculate the inflation rate of the polar cap. However, SuperDARN drift measurements were available only in the longitudinal sector between 14 MLT and 02 MLT. Therefore, attention was focused on calculations of merging in that local time sector.

4.1 SOLAR WIND CONDITIONS

The interplanetary magnetic field, measured by the WIND spacecraft near L1 alternated significant southward IMF B_z periods with brief northward IMF excursions between 12 and 21 UT on 14 February. An extended period of negative IMF B_z occurred between 21:30 UT on 14 February and 02:30 UT on 15 February interrupted only by a brief (~30 min) northward excursion at 22:30 UT (Figure 2). Given the IMF and solar wind speed (averaging 360 kms^{-1}) measured by WIND, the calculated power delivered by the solar wind, defined as the "epsilon" parameter, was ~0.5×10^{18} erg•s^{-1} during the period of weak southward IMF between 20 UT and 21:30 UT. It then reached a nearly constant value averaging 1.0×10^{18} erg•s^{-1} during the steady southward IMF period.

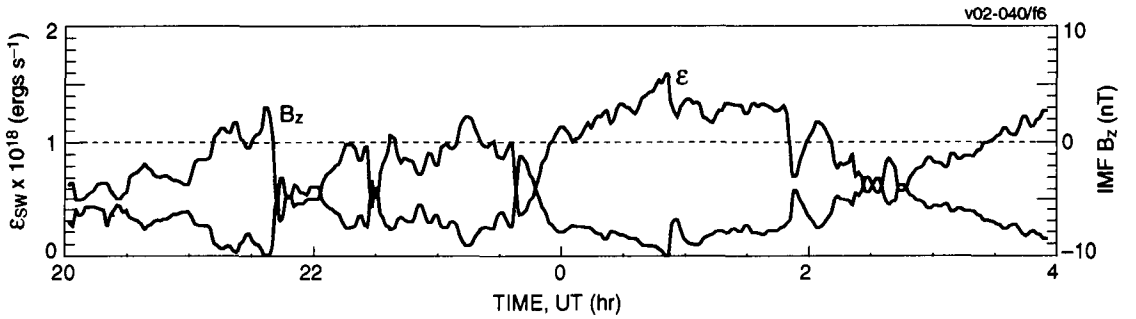

Figure 2. WIND measurement of the Z-GSM component of the IMF and estimated power delivered by the solar wind ("epsilon" parameter) between 2141:37 UT and 2339:08 UT on 14 February 1998. Quantities are time delayed to the subsolar point in the magnetopause.

4.2 AURORAL EVOLUTION

The history of auroral intensifications observed with POLAR UVI (Figure 3) shows that during the period of embedded brief southward IMF intervals between 21 UT and 2235:49 UT, there were several pre-midnight pseudobreakups. The first auroral intensification that evolved into significant propagation started at 2235:49 UT, near the high latitude boundary of the oval in the pre-midnight region. This intensification coincided with the initiation of a rotation of the IMF into a steady negative B_z configuration that lasted five hours (see Figure 2). The region of auroral activity expanded azimuthally after the onset to cover a longitudinal sector 10 MLT hours wide by 2255:13 UT. The oval then developed azimuthal structure consisting of spatially isolated intensifications with an azimuthal separation between 0.5 and 2 h MLT. An azimuthal separation of ~1 h is particularly clear in the pre-midnight sector in the interval between 2322:49 and 2338:09 UT in Figure 3a. If the separation between contiguous arcs is assumed to correspond to the ionospheric image of the azimuthal size of channels of BBFs in the plasma sheet, then the arc separation can be projected to a BBF cross-tail scale size by tracing the magnetic field lines into the plasma sheet using the Tsyganenko 89C model with Kp = 3. This method gives a scale size of 1–4 R_e, consistent with previous estimations of transverse scale length of BBFs [Angelopoulos et al., 1996,1997; Kauristie et al., 1999]. A significant change in the auroral oval morphology was initiated at the maximum epoch of the substorm expansion phase and extended into the recovery phase and SMC portions of the magnetosphere evolution. The change was characterized by polar cap boundary arc intensifications (PBIs) starting with the 2324 UT UVI image. The PBIs extended southward into meridionally elongated auroral structures separated by 0.5 to 2.0 MLT, connecting the poleward and equatorward arcs of the double oval, as shown in the bottom row images of Figures 3a and 3b. These structures have been previously reported and have been interpreted as the auroral images of channels of enhanced convection in the plasma sheet [e.g., Henderson et al., 1998]. The azimuthal separation between PBIs and its projection to a cross-tail scale size will be used in Section 4.5 to calculate the effective contribution of BBF convection to the cross-tail potential.

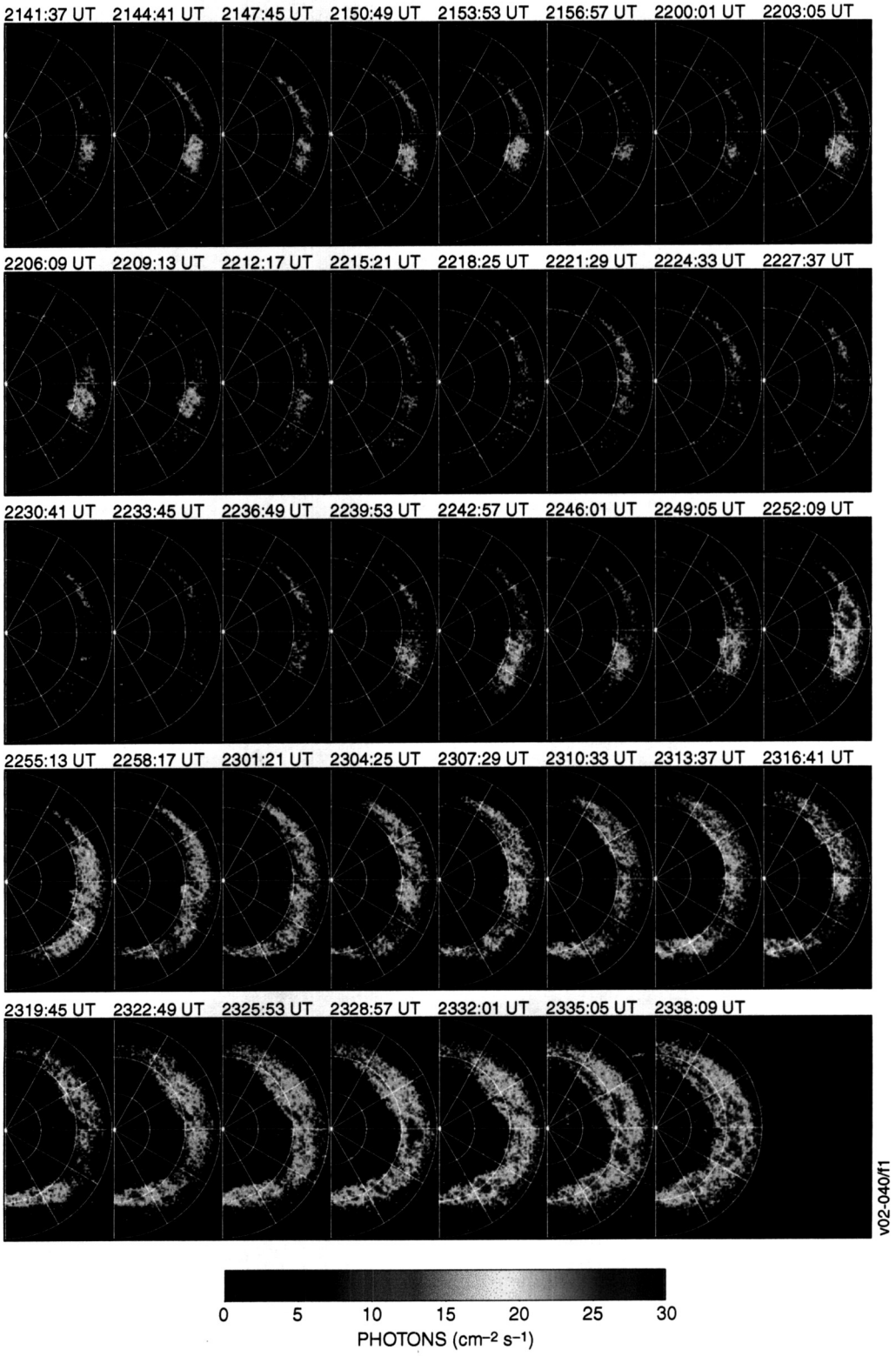

Figure 3a. Evolution of nightside auroral activity between 2141:37 UT and 2338:09 UT on 14 February 1998.

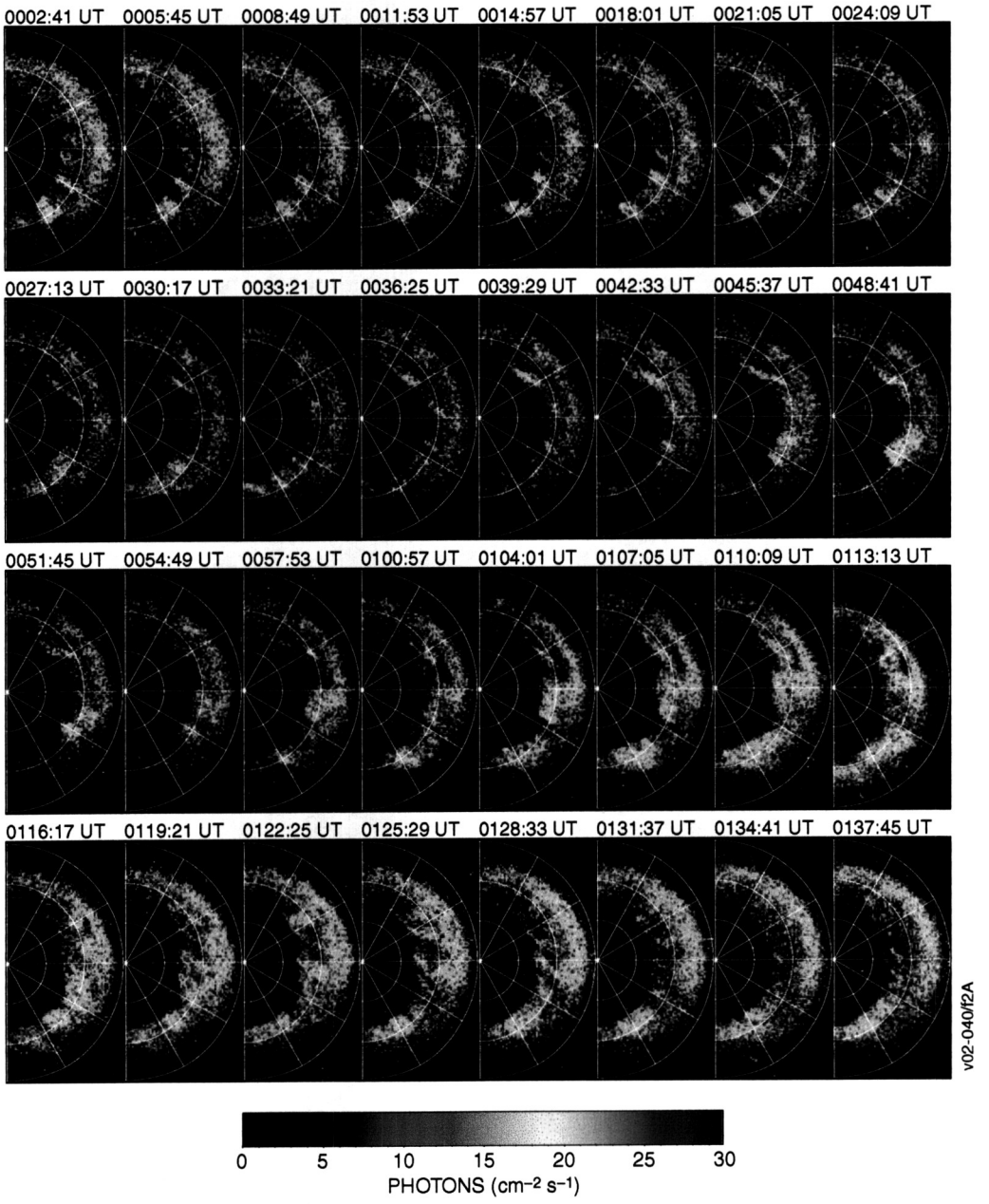

Figure 3b. Evolution of nightside auroral activity between 0002:41 UT and 0137:45 UT on 15 February 1998.

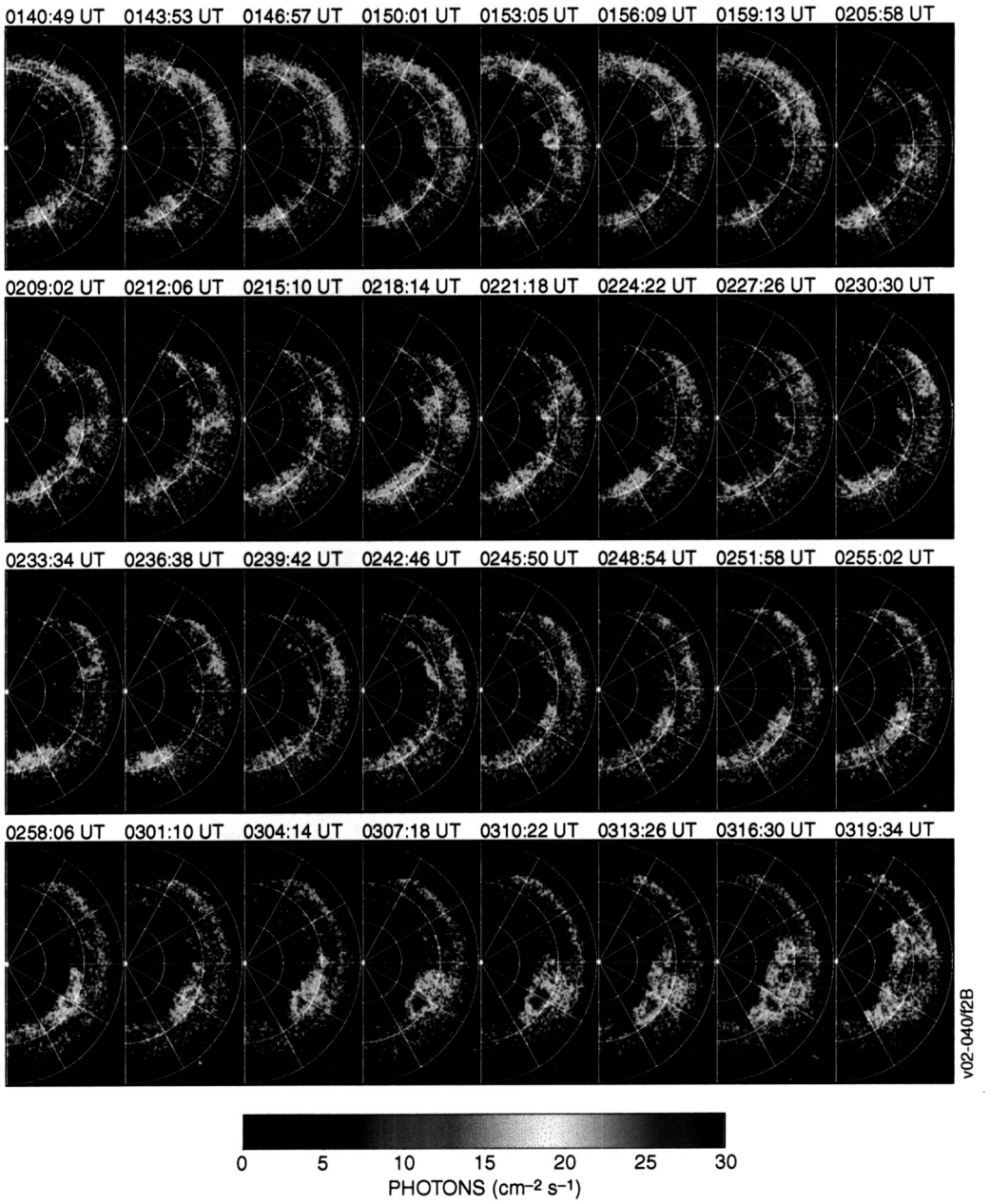

Figure 3c. Evolution of nightside auroral activity between 0140:49 UT and 0319:34 UT on 15 February 1998.

4.3 CALCULATION OF RECONNECTION POTENTIAL

Figure 4 shows a combination of polar cap boundary inferred from POLAR UVI measurements, with ionospheric convection distribution inferred from SuperDarn measurements to calculate the reconnection potential in the frame of reference of the polar cap boundary. The upper left panel in each snapshot shows the detector plane of the UVI instrument. The upper right panel shows the image after correction for scattered sunlight and geomagnetic projection. Superimposed is a fit to the location of the polar cap boundary. The middle panel shows this boundary projected on a two-cell ionospheric electric field distribution and superimposed on the scatter of available SuperDARN measurements (gray scale pixels). The bottom panel shows the magnitude of the reconnection electric field along the polar cap boundary. Red shades indicate positive tangential electric field (net plasma flow into the polar cap), according to the convention illustrated in Figure 1, and blue shades indicate negative values (net plasma flow from the polar cap). The nightside merging potential was calculated by first identifying the local time boundaries of the negative electric field segment of the polar cap boundary and then integrating the electric field between the boundaries.

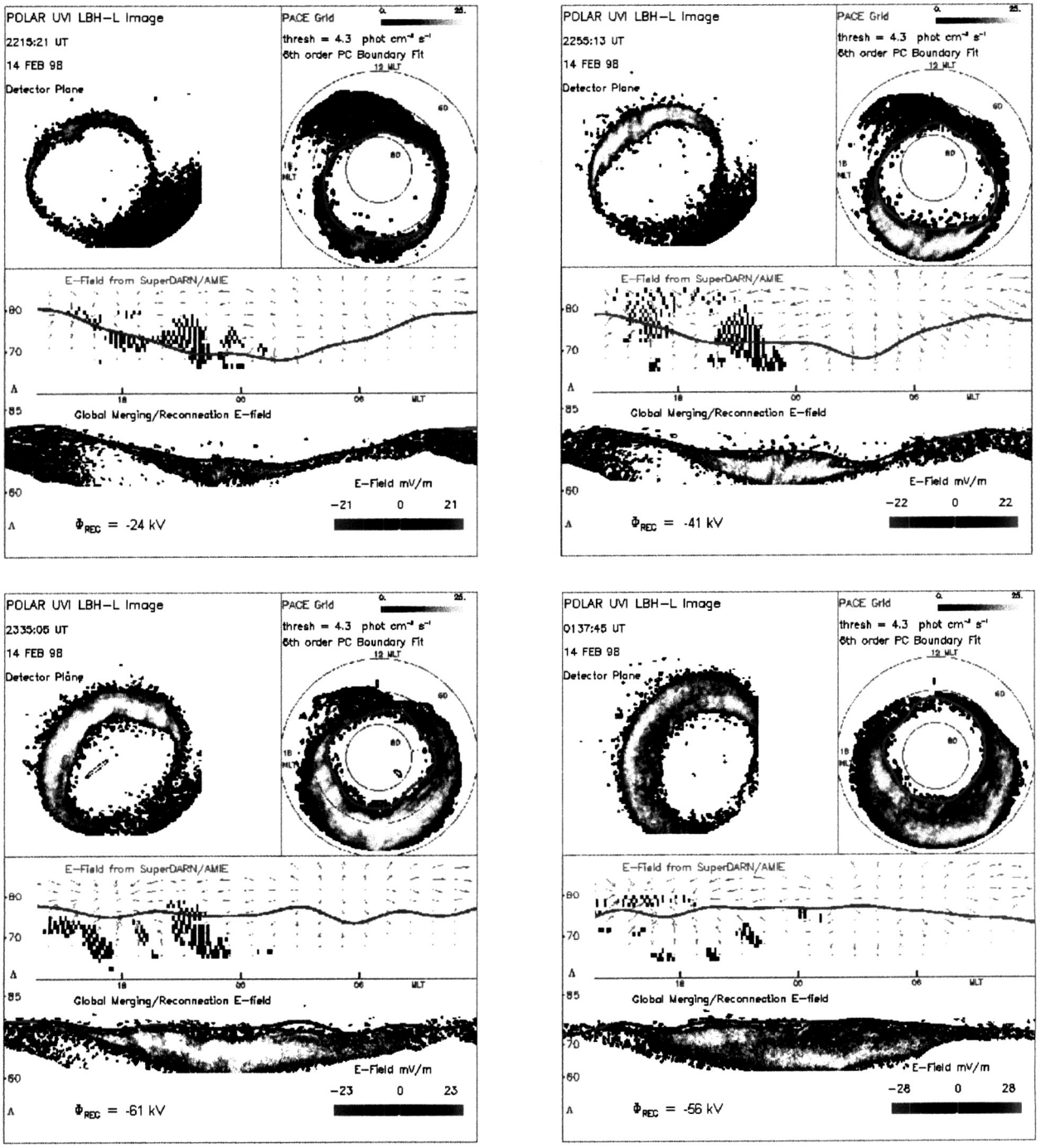

Figure 4. Four snapshots of POLAR UVI and SuperDarn measurements used to calculate the merging potential for 14–15 February 1998.

Figure 5 shows the calculation of nightside merging potential as a function of time and its comparison with the potential inferred from polar cap inflation alone. The top panel shows the evolution of the nightside merging potential calculated between 20 UT on 14 February and 04 UT on 15 February. During the period of pseudo-breakups the merging electric field was on average smaller than 10 mV/m and the reconnection potential was on average smaller than 30 kV. The breakup coincided with the rotation of the IMF into a steady negative B_z configuration that lasted five hours and produced sustained high values of the magnetopause power index "ε" (bottom panel of Figure 5). Auroral activity after the 2235:49 breakup was accompanied by an increase in the electric field to about 20 kV and an increase in reconnection potential to 40 kV at 2255:13 UT, and an electric field above 20 mV/m and a potential of 60 kV at 2335:05 UT. The reconnection potential decreased afterward to 20 kV but increased again with the onset of a so-called polar cap boundary intensification period at 0104:01 UT to 62 kV at 0137:45 UT.

We currently estimate the error in the merging potential due to the uncertainty in the location of the polar cap boundary with a method that uses the arguments of Kauristie et al. [1999] and Baker et al. [2000]. Subsequent to our determination of polar cap boundary location, we simply shift the entire boundary poleward by 3 deg Ë.

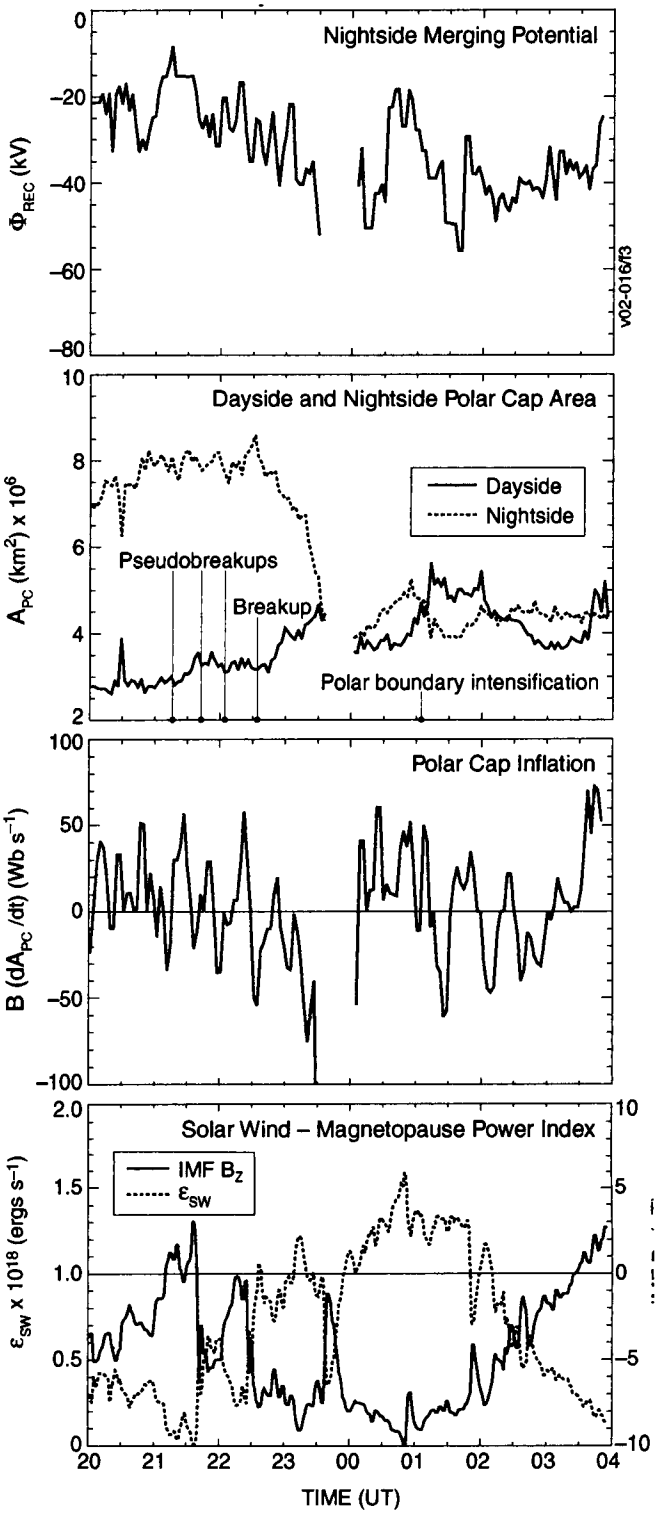

Figure 5. Evolution of nightside merging potential (top panel), polar cap area (second panel), polar cap inflation (third panel), solar wind IMF B_z orientation (red trace at bottom panel), and solar wind power index "ε_{SW}" for 14–15 February 1998.

Figure 6 shows a comparison between the nightside merging potential calculated from the nominal 6th order harmonic fit (red trace) and the merging potential that results after shifting the boundary poleward. As expected, the overall trend is for the potential of the shifted boundary to be stronger. The difference ranges from a few percent to approximately 50% in this example. We will improve the determination of the required amount of poleward shift for those times where there are DMSP passes and or ISR measurements of the polar cap boundary. In the former case, the latitudinal separation between the DMSP boundary (determined from criteria established in Newell and Meng [1988], Newell et al. [1991], and Newell et al. [1996]) and the fitted boundary will dictate the shift to be applied. In the latter case, the polar cap boundary identified from ISR [Blanchard et al., 2001] will be used as the fiducial polar cap boundary. DMSP SSJ4 data files are fully accessible from the JHU/APL data archive. Sondrestrom ISR data are available in our own data archives at SRI International.

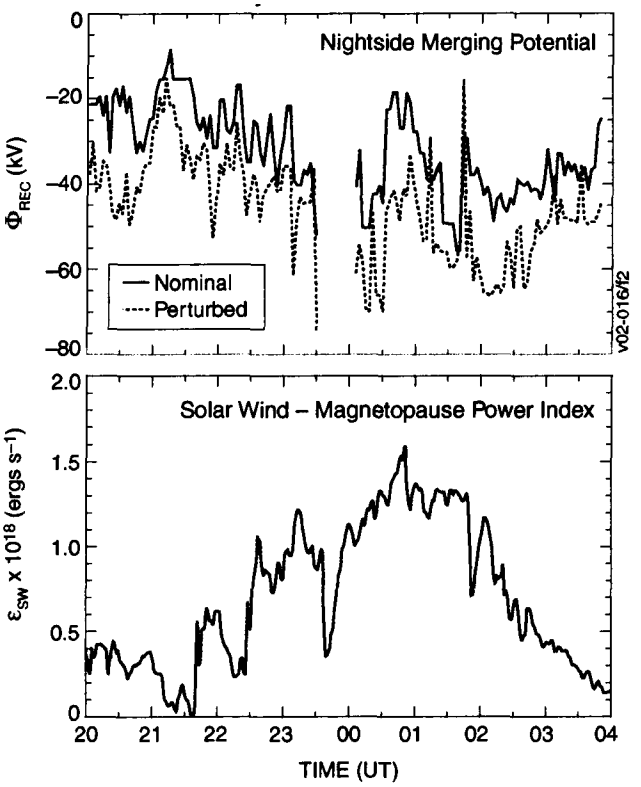

Figure 6. Top panel: Comparison between *nightside merging potential calculated* with a nominal polar cap boundary (red trace) for 14–15 February 1998 and potential calculated with a polar cap boundary displaced 3 degrees poleward. Bottom panel: Solar wind power index "ε_{SW}."

4.4 RELATIONSHIP BETWEEN MERGING RATES AND POLAR CAP INFLATION

The working hypothesis that the net merging rate is the difference between the dayside and nightside merging electric potentials provides an immediate relationship between polar cap size and the net merging rate given by

$$\frac{dr_{PC}}{dt} = \frac{\Phi_D - \Phi_N}{4\pi B r_{PC}} \quad ,$$

where r_{PC} is the polar cap radius, B is the ambient magnetic field in the high latitude ionosphere, and Φ_D–Φ_N is the net merging potential. A comparison of merging rate with the inflation rate of the polar cap can be used to establish a measure of consistency of independent estimates of flux transport across the polar cap boundary and to estimate the deviation of the M–I coupling from steady state for a range of solar wind inputs.

Referring back to Figure 5, the first and third panels of the figure show a comparison of merging potentials with polar cap inflation rate for the 14–15 February 1998 event. In this example, the start of the nightside polar cap deflation coincided with the auroral breakup and a southward turning of the IMF at 22:35 UT (bottom panel). Deflation occurred in two stages. The first stage,

between 22:35 UT and 23:20 UT, occurred at a rate of –50 Wbs^{-1} (equivalent to a merging rate of 50 kV). The second stage, between 23:18 UT and at least the start of the data gap at 23:36 UT, had a much faster deflation rate of -1.0×10^5 Wbs^{-1} (or 100 kV merging rate). Inflation of the dayside polar cap is apparent in the same period of nightside deflation and again at the start of the PBI period (second panel). During the period of PBIs, the nightside merging potential maintained the same strength it had reached during the auroral expansion, but the polar cap did not show the inflation–deflation cycle that was observed with the breakup of 14 February.

4.5 RELATIONSHIP BETWEEN RECONNECTION RATES AND PLASMA TRANSPORT RATE IN THE MAGNETOTAIL

One of the stated main objectives of the project is to quantify the relationship between the potential due to reconnection in the nightside separatrix and the potential due to BBFs defined as flows perpendicular to the magnetic field stronger than 200 km/s and lasting 10 min or less. The correlation is documented in the paper "Measurements of global reconnection in the Earth's magnetosphere: A comparison between substorms and steady magnetospheric convection periods" [Sánchez et al., 2003b]. We quantified the relationship between reconnection rates and flux and plasma transport rate in the substorm–SMC example of 14–15 February 1998. This was a particularly good case to investigate how the reconnection rate versus transport rate relationship changes as a function of solar wind–magnetosphere coupling because in this interval the state of the magnetotail evolved from growth phase to substorm expansion and then settled in a convection bay state. Furthermore, the Geotail spacecraft was very close to the tail axis (X_{GSM} = –29.5 R_e, Y_{GSM} = 1.6 R_e, Z_{GSM} = –1.0 R_e at 00 UT on 15 February) thus allowing direct measurement of convection during extended incursions into the central plasma sheet (defined by $\beta = nkT/(B^2/2\mu) > 0.05$).

Plasma moments from LEP measurements show two periods of earthward BBFs with speeds of up to 1000 km/s between 20 UT and 22 UT on 14 February (Figure 7a). These strong flows occurred despite a weakly negative IMF B_z (see Figure 2), "å" of less than 5×10^{17} ergs s^{-1} and a nightside reconnection potential averaging only 25 kV. In the period between 22 UT and 22:45 UT, total and plasma pressure increased in the central plasma sheet in coincidence with the southward turning of the IMF, "å" increasing to 9×10^{17} ergs s^{-1} and nightside reconnection potential increasing to 35 kV. However, despite the increase in solar wind input and nightside reconnection, BBF activity ceased altogether in the central plasma sheet.

After the 2236:49 UT auroral breakup there was a cluster of earthward-tailward BBFs in coincidence with a bipolar signature in B_z and enhanced magnetic pressure characteristic of the progression of the plasma sheet from growth phase into substorm expansion [e.g., Nagai et al., 1998]. These bipolar flows extended from 22:45 UT to at least 23:25 UT, when Geotail entered the lobe. As Geotail reentered the plasma sheet (23:50 UT), intense earthward BBF activity had replaced bipolar flows (Figure 7b). Nightside reconnection potential increased from 40 kV at breakup to 65 kV at the maximum epoch of expansion (see Figure 6), maintaining this magnitude through 00:30 UT, as "å" increased to 1.3×10^{18} ergs s^{-1}.

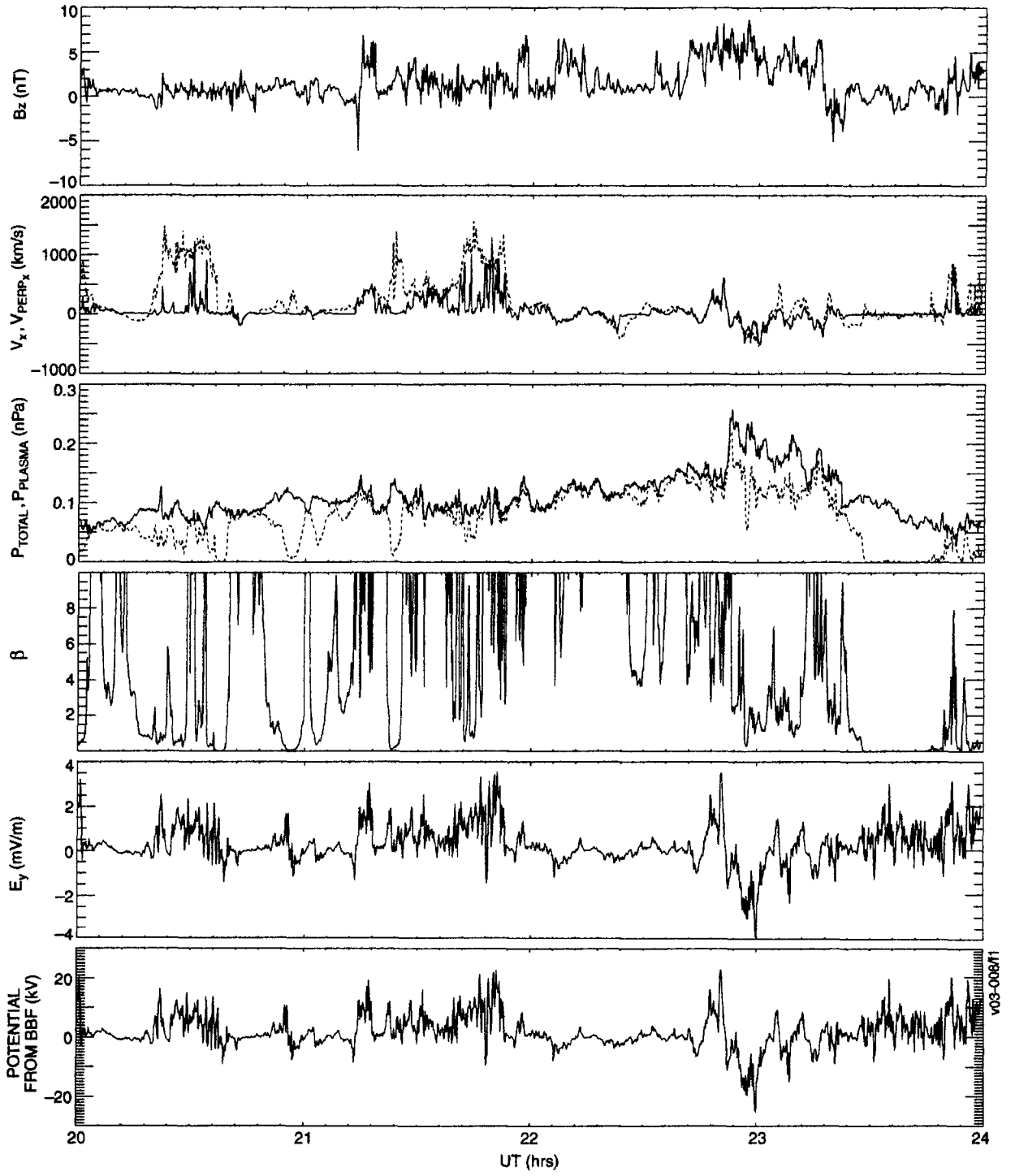

Figure 7a. Geotail plasma and field measurements between 20 and 24 UT on 14 February 1998. Panel 1 shows the GSM component of the magnetic field. Panel 2 shows the X-GSM component of the plasma bulk speed (dashed line) and its projection perpendicular to the local magnetic field. The third panel shows the total pressure (solid line) and the plasma pressure. The fourth panel shows the "beta" ratio of kinetic to magnetic pressure. The fifth panel shows the Y-GSM component of the MHD electric field E = –VxB. The sixth panel shows the contribution of the BBF to the available convection potential assuming a BBF cross-scale size of $1R_e$.

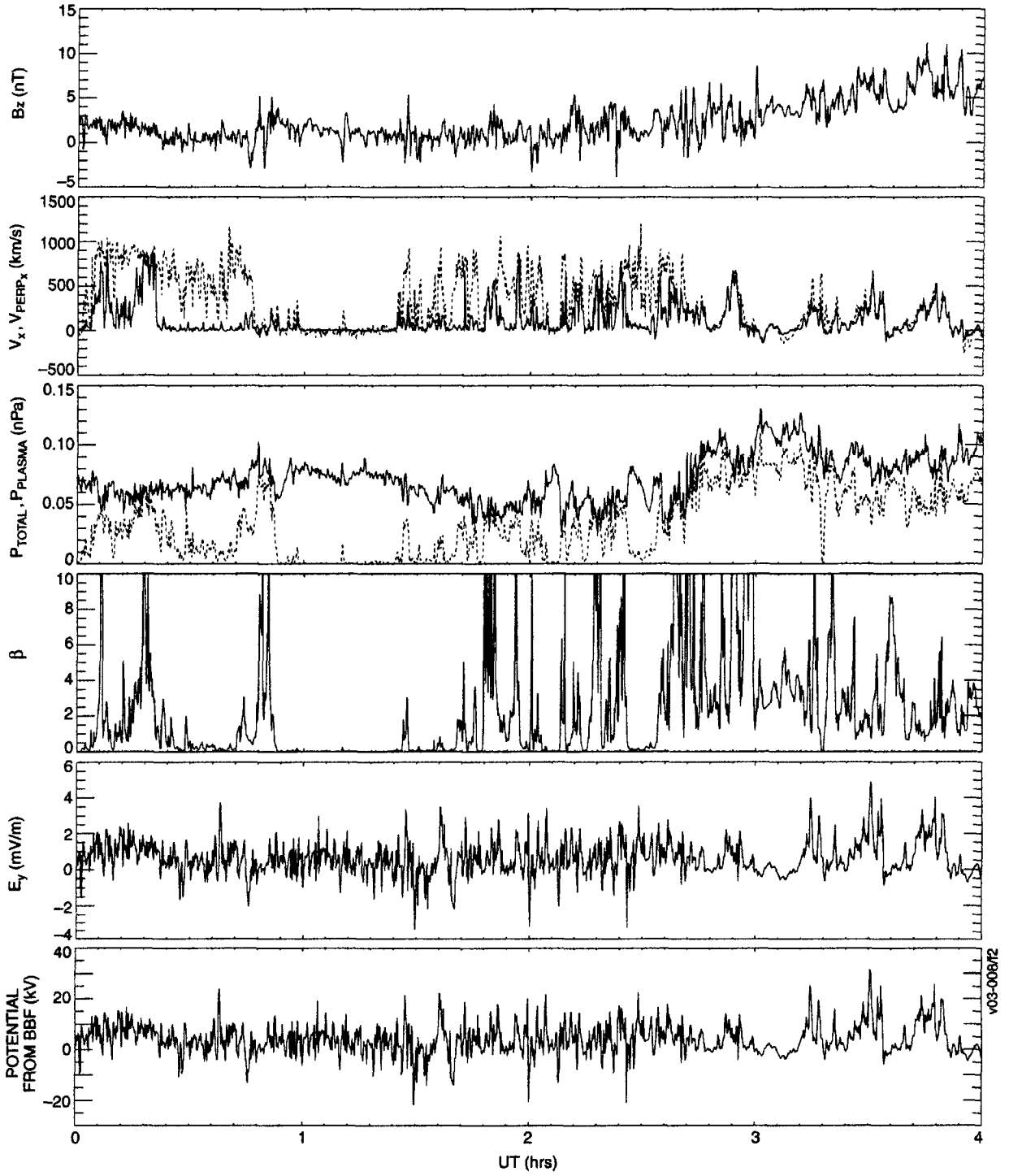

Figure 7b. Geotail plasma and field measurements between 00 and 04 UT on 15 February 1998.The format is the same as Figure 7a.

As expansion and recovery progressed, the oval settled into a smaller polar cap state even though the IMF was in a steady southward orientation that spanned between 00 UT and 03:30 UT on 15 February. During this state the magnetosphere did not develop further substorm activity. Instead, the auroral oval developed PBIs in the pre-midnight sector and into the post-midnight sector from 01 UT onward in coincidence with a dramatic increase in occurrence rate of PBIs (Figures 3b, 3c). During the same period, the occurrence rate of BBFs also increased dramatically in the plasma sheet (Figure 7b). The strength of nightside reconnection potential maintained a slightly smaller average value (50 kV) than the value it had reached at the maximum expansion epoch. This reconnection strength was maintained for the duration of the SMC period with the exception of a decrease between 00:30 UT and 01 UT during which BBF activity ceased completely. Strong convection was reestablished at 01:25 UT and continued uninterrupted through 04 UT.

Note that Geotail entered the lobe even as the polar cap boundary was migrating poleward. Magnetic field line tracing using the Tsyganenko 89C model with Kp = 3 places Geotail's field line footpoint at 100 km altitude in the ionosphere at MLAT = 68.7 deg and MLT = 23.9 h. This location is in the central plasma sheet region of the auroral oval, well below the invariant latitude of the polar cap boundary (75 deg) and between two meridionally elongated auroral arcs, as shown in the sequence of UVI images in Figure 8. The excursion of Geotail into the lobe in a magnetotail flux tube that maps to the low-latitude oval suggests that the BBF channels in the magnetotail are oriented mainly along the tail axis, but are separated from one another by channels of thin plasma sheet.

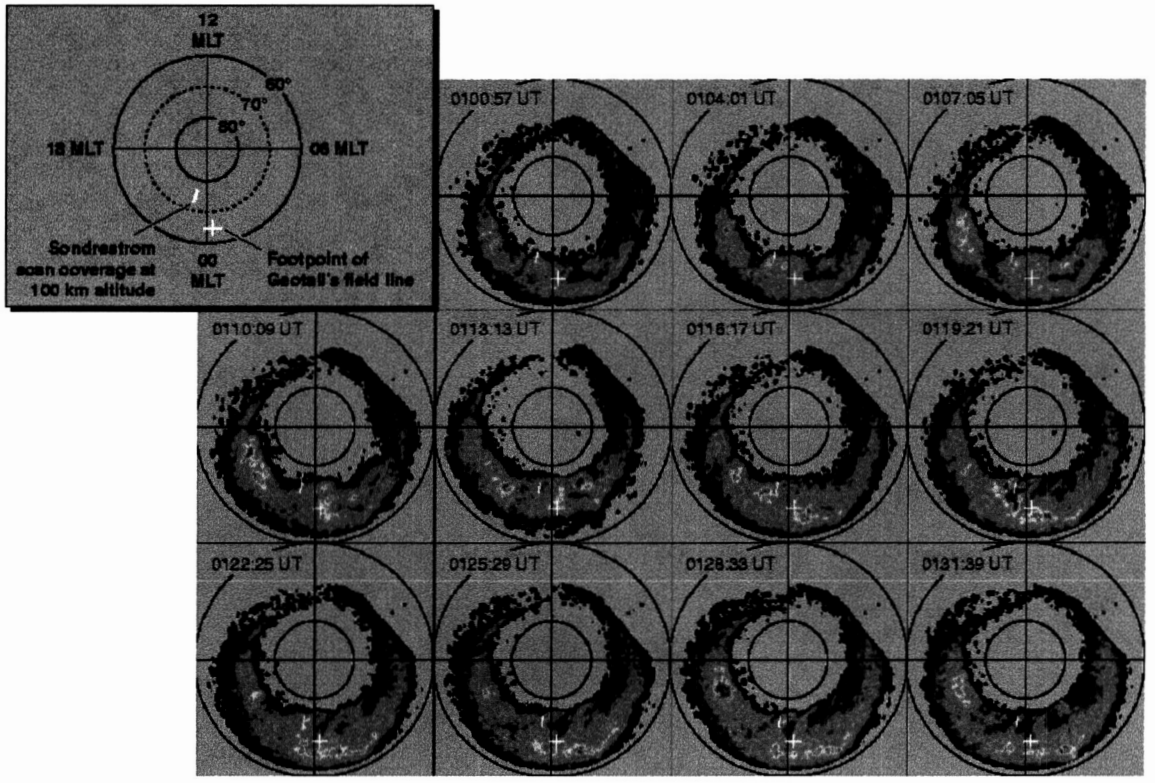

Figure 8. Detail of the arc separation in the oval during BBF activity between 0100:57 UT and 0131:39 UT on 15 February 1998.

A relationship between reconnection and the potential contributed by BBFs was obtained by multiplying the convective electric field with the cross-tail scale of the plasma sheet channels that contain the BBFs. As stated in Section 4.2, the auroral arcs developed azimuthal structure consisting of spatially isolated intensifications with an azimuthal separation between 0.5 and 2 h MLT, with typical azimuthal separation of ~1 h. If the separation between arcs is assumed to correspond to the ionospheric image of the cross-tail scale size of channels of BBFs in the plasma sheet, then the arc separation defines a BBF characteristic cross-tail width of 1–4 R_e. To calculate the cross-tail potential that is expended in driving the BBFs, we simply multiplied the convective electric field (fifth panel of Figures 7a and b) with the cross-scale size of the BBF channels estimated from the auroral projection. The sixth panel of Figures 7a and b show the cross-tail potential assuming a cross-tail scale size of 1 R_e. For the 20–22 UT, the average convection from the BBFs measured by Geotail was between 7 and 15 kV, thus accounting for 30 to 60% of the reconnection potential. This comparison establishes an upper boundary on the number of BBF channels required to carry all the potential to 2 or 3. As the magnetosphere evolved into substorm expansion, the reconnection potential increased to 35 kV, allowing the maximum convection potential of 20 kV, measured at 22:50 UT, to account for 60% of the reconnection potential. As the reconnection potential continued to increase to its maximum measured value of 65 kV at 23:30 UT, the earthward convection potential was only 5 kV which represents a contribution to the total potential of only 8%. In this case convection can still account for a substantial fraction of the reconnection potential if the number of BBFs increases. This requirement appears to be supported by the fact that as substorm expansion proceeded, the region of auroral activity quickly expanded azimuthally.

As the magnetosphere settled into an SMC state the reconnection potential itself settled into a nearly constant value of 50 kV. By comparison, convection measured by Geotail exceeded 10 kV only during substorm recovery and in isolated instances during the SMC period. Its potential was typically ~5%. This behavior suggests that convection occurs in a large number (~10) of azimuthally distributed convection channels in the plasma sheet during most of the time that the magnetotail is in a stable or marginally stable configuration (growth phase and SMC). Coalescence of multiple convection channels into just a few (~2–3) channels is dictated by the migration of the magnetosphere from dynamic stability into an unstable configuration, that is, substorm expansion and recovery.

5 SUMMARY OF RESULTS

The examples shown in this report present the first quantification of the global distribution of the magnetic reconnection rate along the Earth's magnetopause. We have developed a technique that combines POLAR images and ground-based measurements of convection to calculate the rate of magnetic flux transport across the magnetopause for various degrees of magnetospheric coupling to the solar wind. The technique also compares the calculated reconnection rates with the rate of inflation of the polar cap to self-consistency test the assumptions of the method in each individual case.

One of the stated main objectives of the project is to quantify the relationship between the potential due to reconnection in the nightside separatrix and the potential due to BBFs defined as flows perpendicular to the magnetic field stronger than 200 km/s and lasting 10 min or less. We quantified the relationship for the substorm-SMC example of 14–15 February 1998. A relationship between reconnection and the potential contributed by BBFs was obtained by multiplying the convective electric field with the cross-tail scale of the plasma sheet channels that contain the BBFs. The observed relationship suggests that convection occurs in a large number (~10) of azimuthally distributed convection channels in the plasma sheet during most of the time that the magnetotail is in a stable or marginally stable configuration (growth phase and SMC). Conversely, a small number (~2 to 3) of channels appears to be required to account for transport in the magnetotail when it is in an unstable configuration such as substorm expansion and recovery.

The excursion of Geotail into the lobe in a magnetotail flux tube that maps to the low-latitude end of meridionally elongated auroral channels suggests that the BBF channels in the magnetotail are oriented mainly along the tail axis but are separated from one another by channels of thin plasma sheet.

The results of the investigations funded under this project have been reported in three conference presentations and two submissions to the *Journal of Geophysical Research:*

Sánchez, E.R., R.A. Doe, K. Liou, J.M. Ruohoniemi, J.B. Sigwarth, and A.J. Ridley, Autonomous polar cap boundary identification applied to studies of global reconnection rate, *EOS Trans., American Geophysical Union*, 80, p. 883, 1999.

Sánchez, E.R., R.A. Doe, A. T Y. Lui, K. Liou, S. Shepherd, A.J. Ridley, J.B. Sigwarth, and L. Lyons, Reconnection and convection measurements for different degrees of solar wind–magnetosphere coupling, S-RAMP Conference, Sapporo, Japan, October 2000.

Sánchez, E.R., R.A. Doe, N. Fox, K. Liou, and S. Shepherd, Global measurements of reconnection and its relationship to magnetotail transport, *EOS Trans., American Geophysical Union*, 82, p. 1063, 2001.

Sánchez, E.R., R.A. Doe, N. Fox, K. Liou, and S. Shepherd, A new method to measure global reconnection in the Earth's magnetosphere, submitted to *Journal of Geophysical Research*, 2003.

Sánchez, E.R., R.A. Doe, N. Fox, K. Liou, and S. Shepherd, Measurements of global reconnection in the Earth's magnetosphere: A comparison between substorms and steady magnetospheric convection periods, submitted to *Journal of Geophysical Research*, 2003.

REFERENCES

Angelopoulos, V., W. Baumjohann, C.F. Kennel, F.V. Coroniti, M.G. Kivelson, R. Pellat, R.J. Walker, H. Luhr, and G. Paschmann, Bursty bulk flows in the inner central plasma sheet, *J. Geophys. Res., 97*, 4027, 1992.

Angelopoulos, V., C.F. Kennel, F.V. Coroniti, R. Pellat, M. G. Kivelson, R.J. Walker, C.T. Russell, W. Baumjohann, W.C. Feldman, and J.T. Gosling, Statistical characteristics of bursty bulk flow events, *J. Geophys. Res., 99*, 21527, 1994.

Angelopoulos, V., F.V. Coroniti, C.F. Kennel, M.G. Kivelson, R.J. Walker, C.T. Russell, R.L. McPherron, E.R. Sánchez, C.-I. Meng, W. Baumjohann, G.D. Reeves, R.D. Belian, N. Sato, E. Friis-Christensen, P.R. Sutcliffe, K. Yumoto, and T. Harris, Multipoint analysis of a bursty bulk flow event on April 11, 1985, *J. Geophys. Res., 101*, 4967, 1996.

Angelopoulos, V., et al., "Magnetotail flow bursts: Association to global magnetospheric circulation, relationship to ionospheric activity and direct evidence for localization," *Geophys., Res. Lett., 24*, 2271, 1997.

Baker, K.B., and S. Wing, A new magnetic coordinate system for conjugate studies of high latitudes, *J. Geophys. Res., 94*, 9139, 1989.

Baker, J.B., C.R. Clauer, A.J. Ridley, V.O. Papitashvili, M.J. Brittnacher, and P.T. Newell, The nightside poleward boundary of the auroral oval as seen by DMSP and the Ultraviolet Imager, *J. Geophys. Res., 105*, 21267, 2000.

Baumjohann, W.J., G. Paschmann, and C.A. Catell, Average plasma properties in the central plasma sheet, *J. Geophys. Res., 94*, 6597, 1989.

Baumjohann, W.J., G. Paschmann, and H. Lühr, Characteristics of high-speed flows in the plasma sheet, *J. Geophys. Res., 95*, 3801, 1990.

Blanchard, G.T., L.R. Lyons, O. de la Beaujardiere, R.A. Doe, and M. Mendillo, Measurement of the magnetotail reconnection rate, *J. Geophys. Res., 101*,15,265, 1996.

Blanchard, G.T., C.L. Ellington, L.R. Lyons, and F.J. Rich, Incoherent scatter radar identification of the dayside magnetic separatrix and measurement of magnetic reconnection, *J. Geophys. Res., 106*, 8185, 2001.

Cowley, S.W.H., and M. Lockwood, "Excitation and decay of solar wind-driven flows in the magnetosphere–ionosphere system," *Ann. Geophys., 10*, 103, 1992.

Doe, R.A., J.D. Kelly, D. Lummerzheim, G.K. Parks, M. Brittnacher, G.A. Germany, and J. Spann, Initial comparison of POLAR UVI and Sondrestrom IS radar estimates for auroral electron energy flux, *Geophys. Res. Lett., 24*, 999, 1997.

Henderson, M.G., G.D. Reeves, and J.S. Murphree, Are north-south aligned auroral structures an ionospheric manifestation of bursty bulk flows?, *Geophys. Res. Lett., 25*, 3737, 1998.

Kauristie, V., J. Weygand, T.I. Pulkkinen, J.S. Murphree, and P.T. Newell, Size of the auroral oval: UV ovals and precipitation boundaries compared, *J. Geophys. Res., 104*, 2321, 1999.

Lockwood, M., S.W.H. Cowley, and M.P. Freeman, The excitation of plasma convection in the high-latitude ionosphere, *J. Geophys. Res., 95*, 7961, 1990.

Lyons, L.R., T. Nagai, G.T. Blanchard, J.C. Samson, T. Yamamoto, T. Mukai, A. Nishida, and S. Kokubun, "Association between Geotail plasma flows and auroral separatrix disturbances observed by CANOPUS photometers," *J. Geophys. Res., 104*, 4485, 1999.

Nagai, T., T. Mukai, T. Yamamoto, A. Nishida, S. Kokubun, and R. P. Lepping, Plasma sheet pressure changes during the substorm growth phase, *Geophys. Res. Lett., 24*, 963, 1998.

Newell, P.T., and C.-I. Meng, The cusp and cleft boundary layer: Low altitude identification and statistical local time variation, *J. Geophys. Res., 93*, 14,549, 1988.

Newell, P.T., W.J. Burke, E.R. Sánchez, C.-I. Meng, M.E. Greenspan, and C.R. Clauer, The low-latitude boundary layer and the boundary plasma sheet at low altitude: Prenoon precipitation regions and convection reversal boundaries, *J. Geophys. Res., 96*, 21,013, 1991.

Newell, P.T., Y.I. Feldstein, Y.I. Galperin, and C.-I. Meng, "The morphology of nightside precipitation," *J. Geophys. Res., 101*, 10737, 1996.

Reiff, P. H., and J. G. Luhmann, Solar wind control of the polar cap voltage, in *Solar Wind-Magnetosphere Coupling*, edited by Y. Kamide and J. A. Slavin, Terra Scientifica, Tokio, p. 452, 1986.

Ruohoniemi, J.M., and K.B. Baker, Large-scale imaging of high-latitude convection with Super Dual Auroral Radar Network HF radar observations, *J. Geophys. Res., 103*, 20797, 1998.

Ruohoniemi, J.M., and R.A. Greenwald, "Statistical patterns of high-latitude convection obtained from Goose Bay HF radar observations," *J. Geophys. Res., 101*, 21743, 1996.

Sánchez, E.R., R.A. Doe, K. Liou, J.M. Ruohoniemi, J.B. Sigwarth, and A.J. Ridley, Autonomous polar cap boundary identification applied to studies of global reconnection rate, *EOS Trans., American Geophysical Union*, 80, p. 883, 1999.

Sánchez, E.R., R.A. Doe, A.T.Y. Lui, K. Liou, S. Shepherd, A.J. Ridley, J.B. Sigwarth, and L. Lyons, Reconnection and convection measurements for different degrees of solar wind–magnetosphere coupling, S-RAMP Conference, Sapporo, Japan, October 2000.

Sánchez, E.R., R.A. Doe, N. Fox, K. Liou, and S. Shepherd, Global measurements of reconnection and its relationship to magnetotail transport, *EOS Trans., American Geophysical Union*, 82, p. 1063, 2001.

Sánchez, E.R., R.A. Doe, N. Fox, K. Liou, and S. Shepherd, A new method to measure global reconnection in the Earth's magnetosphere, submitted to *Journal of Geophysical Research*, 2003a.

Sánchez, E.R., R.A. Doe, N. Fox, K. Liou, and S. Shepherd, Measurements of global reconnection in the Earth's magnetosphere: A comparison between substorms and steady magnetospheric convection periods, submitted to *Journal of Geophysical Research*, 2003b.

Sergeev, V.A., R.J. Pellinen, and T.I. Pulkkinen, Steady magnetospheric convection: A review of recent results, *Space Sci. Rev., 75*, 551, 1996.

Siscoe, G.L., and T.S. Huang, Polar cap inflation and deflation, *J. Geophys. Res., 90*, 543, 1985.

Torr, M.R., D.G. Torr, M. Zukic, R.B. Johnson, J. Ajello, P. Banks, K. Clark, K. Cole, K. Keffer, G. Parks, B. Tsurutani, and J. Spann, A far ultraviolet imager for the International Solar-Terrestrial Physics Mission, in *The Global Geospace Mission,* Kluwer Academic Publishers, p. 329, 1995.

Vasyliunas, V. M., Steady state aspects of magnetic field line merging, in *Magnetic Reconnection in Space and Laboratory Plasmas,* Geophys. Monogr. Ser., vol 30, edited by E. W. Hones Jr., p. 25, AGU, Washington, D.C., 1984.

GLOSSARY

AMPTE	Active Magnetosphere Particle Tracer Explorer
BBF	bursty bulk flow
DMSP	Defense Meteorological Satellite Program
IMF	interplanetary magnetic field
ISEE	International Sun Earth Explorer
ISR	incoherent-scatter radar
ISTP	International Solar Terrestrial Physics
JHU	Johns Hopkins University
JPL	Jet Propulsion Laboratory
M–I	magnetosphere–ionosphere
MLT	magnetic local time
PBI	polar cap boundary arc intensification
SHF	Spherical Harmonic Fitting
SMC	steady magnetosphere convection
SZA	solar zenith angle
UT	universal time
UV	ultraviolet
UVI	ultraviolet imager